The International Journal of Advanced Manufacturing Technology (2022) 119:2409–2428
https://doi.org/10.1007/s00170-021-08199-5

ORIGINAL ARTICLE

Methodological approach for the development of an operator assistance system for the press shop

Matthäus Kott[1] · Daniel Echler[2] · Peter Groche[3]

Received: 2 July 2021 / Accepted: 10 October 2021 / Published online: 13 December 2021

Abstract
The productivity of a deep drawing process strongly relies on its robustness as well as the experience of the machine operator. Steadily increasing requirements regarding weight, design and efficiency lead to a production operating increasingly closer to the process limits, making it more challenging to ensure a high robustness of the process. Minimal process fluctuations caused by disturbances such as varying material properties or changing tribological conditions may negatively affect the process due to deteriorated product properties as well as an increased risk of scrap. Thus, a target-oriented adjustment of available parameters by the machine operator becomes more difficult, and an increased knowledge about the causes of defects is more important. In the past, several approaches with different combinations of sensors and actuators have been investigated to enable a stable process window based on a control system. This paper presents a method to address the need for a more robust process by developing an operator assistance system that enables the identification of the component state and provides decision support to the machine operator. The methodological approach includes a thorough process analysis to evaluate the expediency of such a system and to make a reasonable preselection of sensors in order to avoid unnecessary costs.

Keywords Variant simulations · Sensitivity analysis · Neural networks · Decision-making · Assistance system

1 Introduction and state of the art

The body-in-white represents about 40% of the total vehicle weight making it the heaviest element of modern conventional vehicles. The consequent application and implementation of modern lightweight measures appears to be very effective and is of crucial importance for weight reduction in the vehicle production to ensure sustainable and financially affordable mobility as well as the competitiveness of a car manufacturer [1, 2]. To achieve these goals, in addition to the use of innovative multi-material concepts and multiphase steels, steadily decreasing wall thicknesses combined with complex part geometries and high production rates are pursued [3]. The overall complexity of this challenge is intensified by increasing requirements for stiffness, acoustics and crash performance, which are usually in conflict with principles and strategies of modern lightweight design [2]. Hence, deep drawing processes of car body parts are operated closer and closer to the process limits, which increases the challenge to ensure stable processes with high robustness [4]. Conditions of uncertainty as well as a lack of knowledge of the process may lead to deteriorated product properties and part failure resulting in a diminished productivity [5]. In particular, the influence of increasing tool temperatures on tribological conditions [6] as well as disturbances with stochastic fluctuations such as material properties [7] affect the deep drawing process. In the past, several approaches using different combinations of sensors and actuators have been investigated to meet the requirements for a more robust process. Purr et al. [8] are gathering data from different measurement systems implemented in a blanking line with the goal of identifying appropriate settings of the stamping line for each metal sheet prior to the start of production in order to obtain deep drawn parts of acceptable quality. For this purpose, the mechanical properties, the thickness and the roughness as well as the thickness of the oil layer of

✉ Matthäus Kott
matthaeus.kott@ptu.tu-darmstadt.de

[1] Opel Automobile GmbH, Bahnhofplatz 1, 65423 Rüsselsheim, Germany

[2] University of Applied Sciences Wiesbaden Rüsselsheim, Am Brückweg 26, 65428 Rüsselsheim, Germany

[3] Technische Universität Darmstadt, Institute for Production Engineering and Forming Machines, Otto-Berndt-Str. 2, 64287 Darmstadt, Germany

the sheet metal are measured inline and analysed using data mining methods to track fluctuations of the sheet metal and their potential influence on the stamping process.

The most common approaches are based on a closed- or open-loop control system that uses sensor data from the stamping process as control variables. The concept of the systems mainly distinguishes between a part-to-part control [9] and the control during the stroke [10], depending on the available actuators and sensors. These systems are also referred to as off-line closed-loop control and on-line closed-loop control systems, following Allwood et al. [5]. In addition to measuring process forces as well as first-order wrinkles [10], most control systems rely on the inline data acquisition of the flange draw-in of the deep drawn part. In one of the first approaches, the flange draw-in has been measured by a linear variable differential transformer (LVDT). The target force of the blank holder could be accomplished by the application of a PI controller using a control algorithm based on the draw-in [11, 12]. Comparable approaches use target curves and envelopes derived from draw-in measurements of reference parts to set up a closed loop control system that manipulates the binder force [10] or the force distribution [13].

Since material flow is one of the few measurands that allows conclusions to be drawn regarding part quality during and after the forming process [6], its measurement methods have been investigated and improved. Tactile displacement transducers [11] and their adaptation by a sheet metal tongue [10] do not appear to be suitable for series production due to the risk of jamming. Thus, inductive sensors withstanding the harsh conditions of the production environment have been developed to investigate the draw-in of the sheet metal part [14]. Recently, however, optical measurement systems have been preferred, although there is a risk of contamination by oil or dust, which may lower their operational suitability. Camera-based systems are able to capture the skid-line distance to the part flange [15] as well as the local material flow [16] and allow the measurement of the global blank draw-in [17] or at least large parts of the global blank draw-in [18]. While these systems are only able to detect the final state of the drawn part and neglect the draw-in curve, laser displacement sensors can overcome this shortcoming and may be an alternative [13]. Although several reliable data acquisition methods are available and control systems have been extensively investigated at laboratory [10, 13, 19] and production scale [9, 20, 21], a thorough preceding process analysis evaluating the expedience of a control system in series production is often simplified. Furthermore, the application of alternative concepts in metal forming such as decision-making assistance systems is widely disregarded and neglected. In [22], an assisted setup for calculating optimal start settings for deep drawing with progressive tools based on multiple quadratic regression models is presented. A more generic approach to assistance systems in forming technology applied to a roll forming process is introduced in [23]. However, the approaches are either specific or general to such a high degree that they do not provide an adequate basis for the application in deep drawing of car body parts.

This paper presents a method for developing an operator assistance system that allows the component state to be detected and provides decision support to the machine operator. The decision-making assistance offers recommendations regarding the optimal settings to manipulate the local material flow and prevent part failure using newly designed adjustable spacers. A prior thorough and systematic process analysis using variant simulations and experimental data allows to assess the expediency of the application of an assistance system, including the preselection of appropriate sensor technologies. Different modelling approaches of selected quality criteria based on variant simulations considering various levels of complexity are discussed regarding their accuracy and suitability for a further analysis. A deep drawn car body part as application example is analysed in terms of its sensitivity to changes in disturbance variables considering first-order and higher order effects. Potential measurands are determined by the maximum achievable observability of part quality criteria that cannot be directly measured. The process analysis is complemented by the evaluation of the process robustness and investigation of the process controllability.

2 Methodological approach

An operator assistance system is not beneficial and can cause unnecessary costs if the process is sufficiently robust. Therefore, a thorough and systematic process analysis is advisable to evaluate the expediency and to make a reasonable preselection of sensors. The schematic for the process analysis as first part of the methodological approach is shown in Fig. 1. Every step is either based on experimental data, data from a numerical simulation and its variants or a combination of both.

The component to be analysed should either be ready for production or at least be in an advanced stage of tryout. Preseries tools at an early stage of tryout are constantly being adjusted and can affect the results of the process analysis. Once a component has been selected, disturbing variables of the process and their variation ranges, probability distributions per parameter as well as the correlations between the parameters have to be determined. Typical disturbances of deep drawing processes are discussed in [24]. After a numerical baseline simulation of the corresponding process has been set up and validated, variants of the simulation are generated by a design of experiments (DoE) using a Latin hypercube sampling under consideration of the information

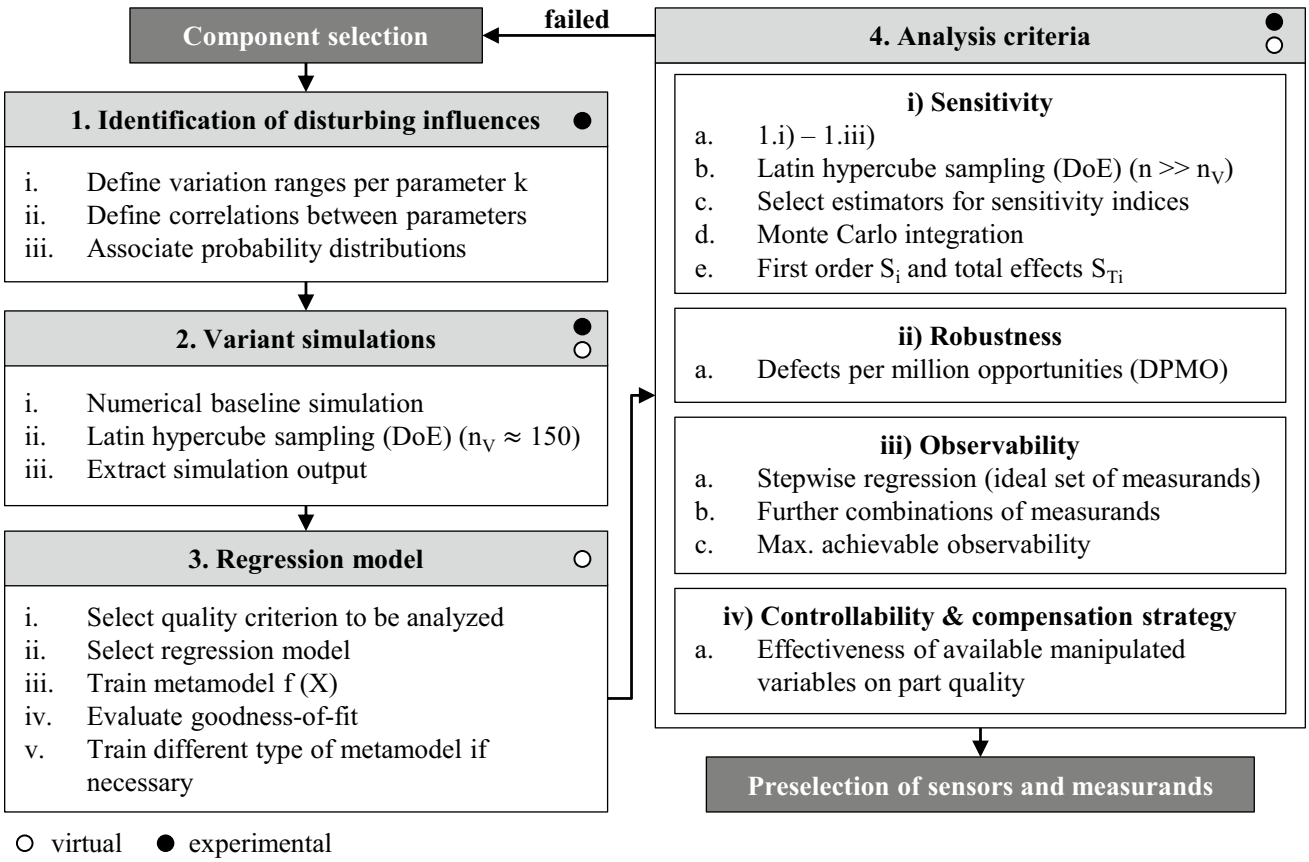

Fig. 1 Schematic of the process analysis

from the first step. The results gained from the variant simulations are used to train several regression models, depending on the achievable goodness-of-fit per model as well as the input and output parameters needed for the process analysis. A variance-based sensitivity analysis taking into account first-order and higher order effects allows the investigation of the most influential input parameters on a selected quality criterion (output). The robustness of the process is evaluated using defects per million opportunities (DPMO) to determine the effectiveness of the process. The analysis of the maximum achievable observability taking into account different combinations of measurands ensures a preselection of sensors that offer benefit for the assistance system. The analysis of the controllability and the derivation of a compensation strategy can be done either experimentally or virtually by numerical simulations. The same applies to the evaluation of robustness, whereby the sensitivity and observability analyses are performed virtually on the basis of the results from the variant simulations, since a sound experimental data basis is usually not available.

The selection of another component is strongly recommended if the process is sufficiently robust, not observable or not controllable. The process analysis is followed by the specific selection of sensor technologies and implementation of the measurement system considering functional, structural and economic criteria (Fig. 2). This step is strongly specific, depending on economic factors and resources as well as the basic conditions in the press shop and the press line. The operator assistance system consists of a process monitoring and a decision-making assistance, as shown in Fig. 3. Changes of the process state due to disturbances are detected by suitable sensor technologies and processed by the assistance system. The machine operator evaluates the information provided and acts at his own discretion, using available actuators to stabilize the process if necessary. The identification of the component state makes it possible to determine whether and in which area the component is critical, based on the analysis of previously recorded measurement data from series production. The results of an experimental setup under consideration of varied manipulated variables make it possible to model a relationship between the control variable and the adjustment of an actuator. This model enables a decision support for the machine operator by offering recommendations on how to set process parameters to prevent part failure. The implementation is completed after a successful proof of concept in series production.

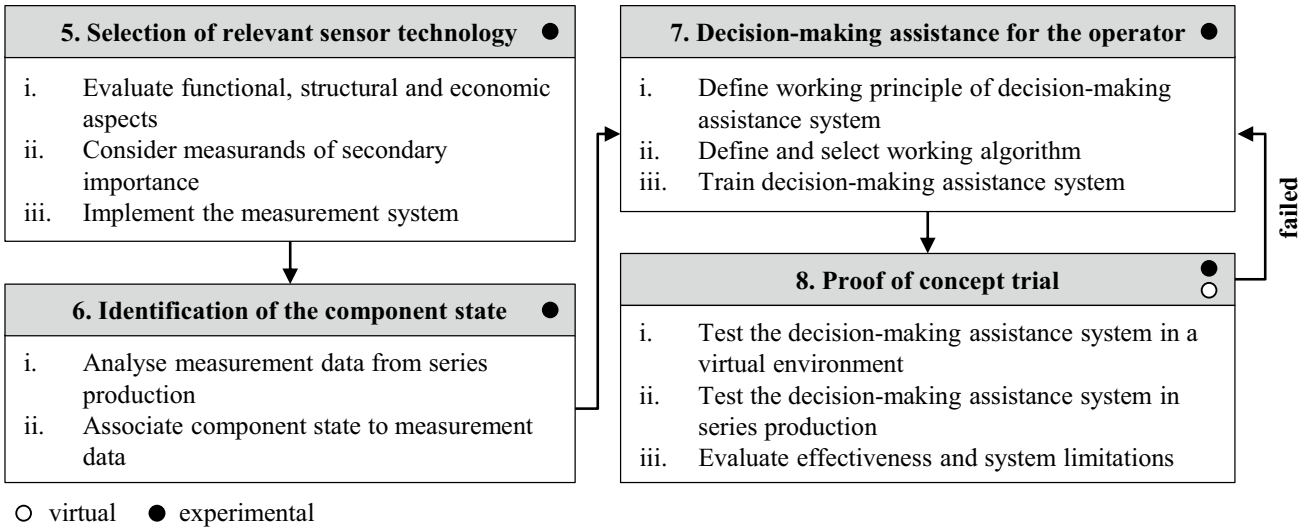

Fig. 2 Schematic of the implementation

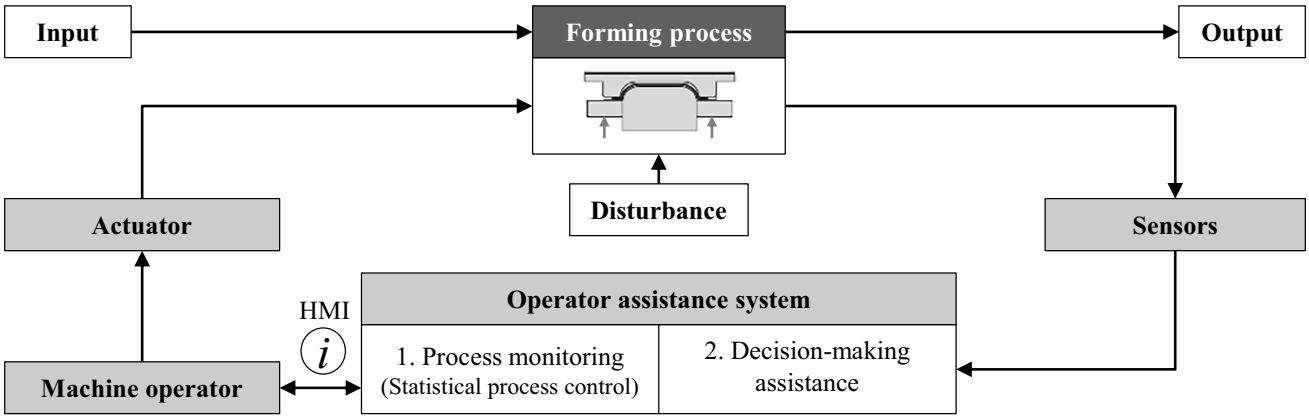

Fig. 3 Concept of the operator assistance system

3 Application example and variant simulations

The spare wheel well of a passenger car was chosen as an application example for this work. It is a double part with a drawing depth of 225 mm made from a hot-dipped galvanized bake hardening steel (CR180B2) in four operations, starting with one drawing operation, followed by two trimming operations and one flanging operation. Since forming is performed close to the process limits in terms of formability, quality issues are mainly limited to necking and tearing in the rib of the part as well as flange wrinkles that can occur during the drawing operation (Fig. 4). Surface defects caused by particles of zinc coating or imprints due to trim waste may appear in rare cases, whereas scrap due to dimensional deviations caused by springback has not been reported in production and will be compensated for by global and local overbending of the parts in the trimming and flanging operation.

The behaviour of the part when any material or process parameter changes is assessed by variant simulations of a numerical baseline simulation. The DoE is generated by Latin hypercube sampling, using 175 simulations based on ESI's commercial finite element software Pam-Stamp. The nominal values of the baseline simulation and the variation ranges of its variants can be seen in Table 1. The results from uniaxial tensile tests were used for the material modelling.

The baseline simulation uses a flow curve approximated as proposed by Swift/Krupkowsky [25] and a Vegter 2017 [26, 27] yield locus. The forming limit curve (FLC) has been determined by Nakajima tests [28], whereas the Keeler-Goodwin approach [29, 30] has been used for the variants.

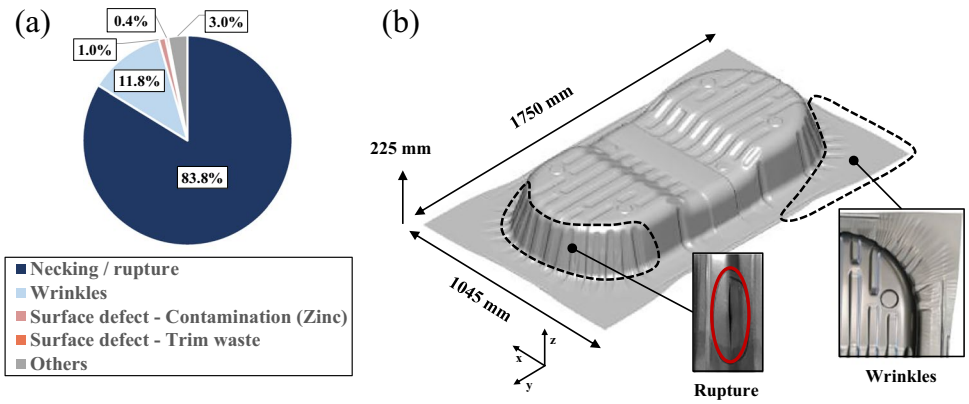

Fig. 4 Quality issues of the spare wheel well after 98,494 produced parts (**a**) and first operation including main type of defects (**b**)

The tool surfaces in the simulation were derived from 3D scans of the real tooling using a GOM Atos system. Since the variation range of each parameter should correspond to the variation range to be expected in series production in order to avoid an over- or underestimation of parameters [31], several offline measurements were carried out in advance for the application example. The variation range of each parameter was derived from results of 936 uniaxial tensile tests, considering 35 coils in total. The sheet thickness is deduced from inline measurements in the coil line, while the constant friction coefficients were estimated based on strip drawing tests considering different tool temperatures (20–60 °C), contact pressures (2–10 MPa) and sliding velocities (10–300 mm/s).

The baseline simulation is validated by the draw-in of two digitized parts scanned by a GOM Atos system and a full-field strain analysis carried out by a Vialux Autogrid-comsmart device. The deviations in the flange draw-in between the digitized parts and the numerical simulation for 20 positions are shown in Fig. 5. All positions are arranged uniformly but not symmetrically, except for positions 3 and 13 as well as 8 and 18. The numerical simulation meets the real parts very well in terms of flange draw-in.

A maximum deviation of + 5.5 mm is observed for position 18, whereas the deviation is significantly lower for most other positions. A full-field strain analysis after the forming process as second validation criterion requires marking the sheet metal with a squared grid pattern. Electrolytic marking with a 2.5 mm grid and one-point coding was used. The comparison of the thinning behaviour between the numerical simulation and the part from series production is shown in Fig. 6. Gaps in the digitized part result from the size of the stencil. The component was divided into 20 measurement areas, which were reassembled at the end. As before, the results of the numerical simulation are close to the experimental data, and no large discrepancies can be detected between the simulated and measured thinning.

In general, differences in the draw-in behaviour and thinning distribution are a result of simplifications within the simulation. This includes the constant friction coefficient, the consideration of rigid tools neglecting elastic behaviour and the non-consideration of a mixed isotropic-kinematic hardening in particular. However, the baseline simulation can be considered as suitable operational point for the variant simulations due to its high conformity with the measurements.

Table 1 Parameters and its ranges for the variant simulations

Parameter	Nominal value	Variation range
Friction coefficient	0.08	0.06–0.12
Blank thickness	0.65 mm	0.618–0.673
Yield strength	212 MPa	181–244 MPa
Tensile strength (0°)	322 MPa	301–336 MPa
Tensile strength (45°)	334 MPa	309–347 MPa
Tensile strength (90°)	320 MPa	301–333 MPa
r value (0°)	2.27	1.49–3.42
r value (45°)	1.57	1.06–2.04
r value (90°)	2.49	1.38–3.99
Uniform elongation (0°)	20.02%	19.41–22.62%
Uniform elongation (45°)	17.67%	16.80–20.21%
Uniform elongation (90°)	19.17%	18.49–21.50%
Strain hard. exp	0.196	0.159–0.216
x-position blank	0 mm	± 2.5 mm
y-position blank	0 mm	± 2.5 mm

4 Setup of regression models

The results extracted from the variant simulations enable the estimation of a relationship between k independent variables such as the varied parameters X_i and a dependent variable Y, which may represent a quality criterion as a function of the independent variables $Y = f(X)$. Simulation-based regression models are often referred to as metamodels and can be

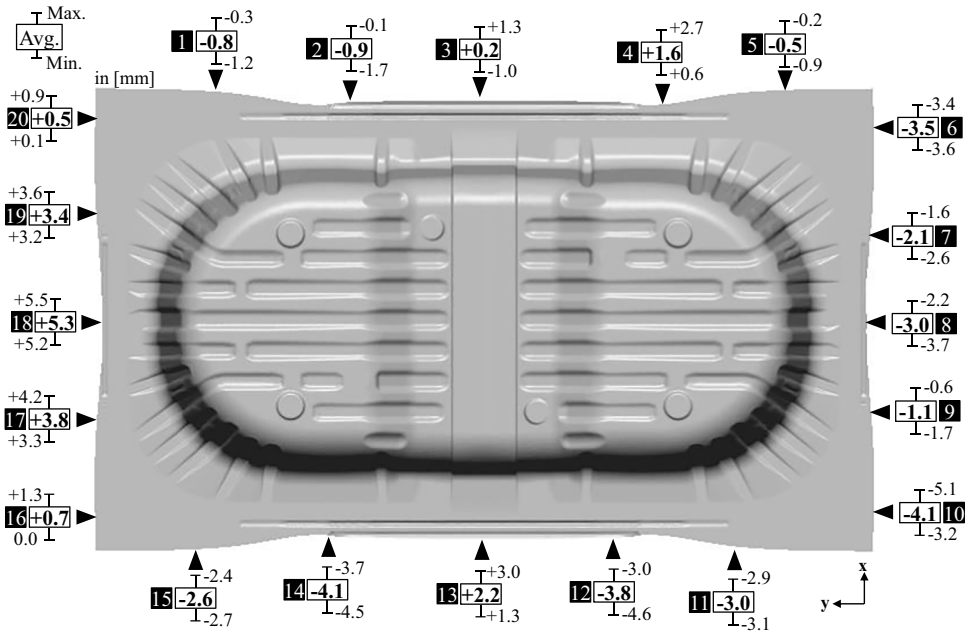

Fig. 5 Absolute deviation of the flange draw-in between digitized part and baseline simulation

calculated by a large variety of approximation or interpolation approaches. Especially in forming technology, either the approximating response surface methodology (RSM) such as multiple linear regression (MLR) or multiple quadratic regression models (MQR) (including or excluding interaction terms) [32] and interpolating approaches such as radial basis functions (RBF) are widely used [33, 34]. Recently, however, machine learning approaches have been increasingly pursued since they allow to approximate even complex non-linear relationships. In the present work, the established RSM and RBF models are applied to calculate the quality criteria rupture risk derived from the forming limit diagram (FLD) as well as the wrinkling ε_{wc}. The latter is based on the evaluation of the strain state to detect wrinkles and depends on the average anisotropic exponent R as well as the major strain ε_1 and minor strain ε_2 [35]:

$$\varepsilon_{wc} = \max\left[-\left(\varepsilon_2 + \frac{R}{1+R}\varepsilon_1\right), 0\right] \tag{1}$$

Both criteria represent the main quality issues of the application example. The regression results are compared with the two popular machine learning approaches support vector regression (SVR) and multilayer artificial neural networks (ANN) in terms of their coefficient of determination (R^2) considering a sevenfold cross-validation, as shown in Table 2. As a consequence, approximately 15% of the data set of 175 simulations is used as independent test data. Multiquadric RBF's were used for both quality criteria providing the highest goodness-of-fit compared to the cubic, thin plate

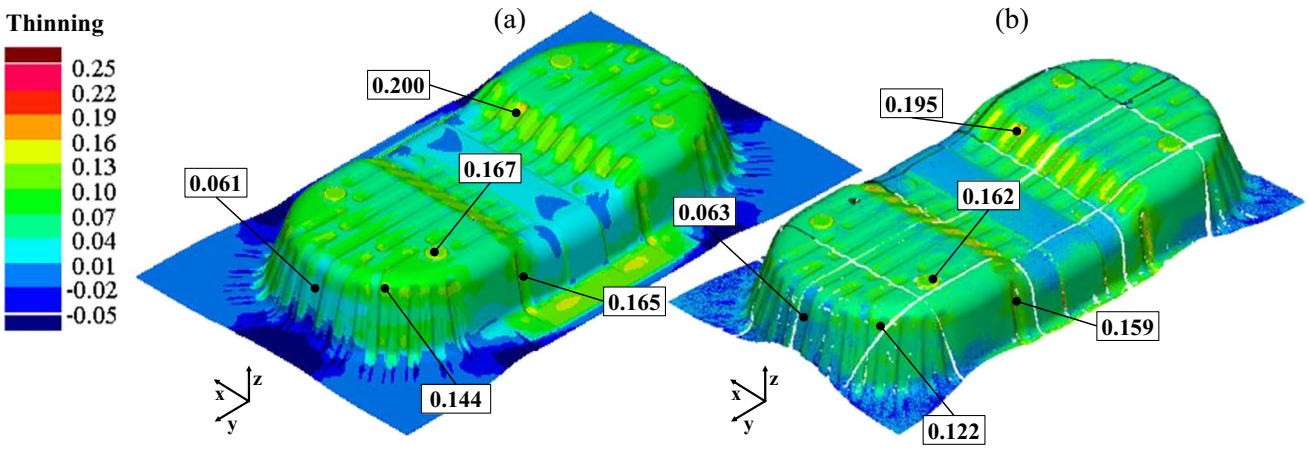

Fig. 6 Comparison of the thickness reduction between simulation (**a**) and digitized part (**b**)

Table 2 Maximum achieved coefficients of determination regarding different modelling approaches

Model type	R^2	Rupture risk	Wrinkling
1) Multiple linear regression (MLR)	R^2 Train	92.96%	97.95%
	R^2 Test	91.66%	96.28%
	R^2 All	92.80%	96.90%
2) Multiple quadratic regression incl. interactions (MQR)	R^2 Train	96.24%	99.69%
	R^2 Test	94.35%	87.48%
	R^2 All	96.03%	95.93%
3) Radial basis function (RBF)	R^2 Train	100.00%	100.00%
	R^2 Test	3.98%	5.88%
	R^2 All	80.34%	81.49%
	Type	Multiquadric	Multiquadric
4) Support vector regression (SVR)	R^2 Train	92.86%	97.88%
	R^2 Test	90.41%	96.32%
	R^2 All	92.61%	97.28%
	Kernel	Linear	Linear
5) Multilayer artificial neural networks (ANN)	R^2 Train	99.40%	98.16%
	R^2 Val	95.40%	96.12%
	R^2 Test	95.47%	98.59%
	R^2 All	**97.94%**	**97.44%**
	Neurons	[10; 16; 16]	[10; 10]

spline, inverse multiquadric, inverse quadric or Gaussian RBF types. For the SVR models, a linear kernel provided best results compared to a quadratic, cubic or Gaussian kernel.

Finally, the neural networks are calculated using the Levenberg–Marquardt algorithm [36] considering 70% training data and 15% validation data. Each hidden layer contains 10 to 60 neurons, and the depth of the neural networks is limited to four hidden layers. The calculation is terminated once a depth of four hidden layers and 60 neurons per layer or a minimum R^2 of 86.5% is reached for the training, validation and test phase. This termination criterion is necessary since artificial neural networks, in contrast to the model types 1–4, are not deterministic in terms of the global optimum achieved.

The results indicate that comparatively less complex models such as the MLR or MQR including interaction terms already provide a high goodness-of-fit and robust results regarding the approximation of the selected quality criteria. The same applies to the SVR models with all R^2 above 90%. Thus, these models would be suitable for further analysis. However, the ANN models appear to be the most reliable and robust regarding the estimation of the rupture risk and wrinkles of the application example, although their calculation is the most expensive one. RBF models are the least suitable for the present cases. The high deviation between the R^2 of the training and test data implies a strong tendency to data-overfitting.

Table 3 Radial design of the re-sample matrix $\boldsymbol{A}_{\boldsymbol{B}}^{(i)}$

Step	Sampling
$\boldsymbol{A}$	$a_{11}, a_{12}, a_{13}, \ldots, a_{1k}$
$\boldsymbol{A}_{\boldsymbol{B}}^{(1)}$	$b_{11}, a_{12}, a_{13}, \ldots, a_{1k}$
$\boldsymbol{A}_{\boldsymbol{B}}^{(2)}$	$a_{11}, b_{12}, a_{13}, \ldots, a_{1k}$
$\boldsymbol{A}_{\boldsymbol{B}}^{(3)}$	$a_{11}, a_{12}, b_{13}, \ldots, a_{1k}$
…	…
$\boldsymbol{A}_{\boldsymbol{B}}^{(k)}$	$a_{11}, a_{12}, a_{13}, \ldots, b_{1k}$

5 Evaluation of the process

The implementation and application of an operator assistance system does not necessarily offer advantages in terms of productivity for every deep drawing process in series production. Thus, a systematic process analysis considering key criteria that need to be met for an expedient operation is beneficial to avoid unnecessary costs. In addition, the selection of suitable sensor technologies is becoming increasingly important when such solution approaches are being considered, especially since quality criteria in deep drawing are only measurable with great effort, so that substitute measurands are generally indispensable for efficient inline measurements.

5.1 Variance-based sensitivity analysis

Sensitivity analysis allows the identification of parameters with the highest influence on a predefined dependent variable, such as main failure modes and quality criteria, leading to a deeper understanding of the process. Especially

Table 4 Standardized Sobol indices for rupture risk and wrinkling

		Rupture risk		Wrinkling	
					
Parameter		**1. Order**	**Total**	**1. Order**	**Total**
Friction coefficient		82.5%	70.9%	61.1%	69.5%
Blank thickness		0.5%	0.7%	1.4%	0.2%
Yield strength		0.3%	0.8%	2.8%	2.3%
Tensile strength (0°)		0.0%	1.6%	3.1%	2.9%
Tensile strength (45°)		0.2%	0.9%	1.5%	1.0%
Tensile strength (90°)		1.3%	2.3%	2.1%	1.9%
r-value (0°)		0.2%	1.4%	1.7%	1.1%
r-value (45°)		0.0%	1.9%	3.4%	4.1%
r-value (90°)		0.2%	1.3%	9.8%	9.9%
Uniform elongation (0°)		0.3%	2.0%	1.3%	0.4%
Uniform elongation (45°)		0.8%	1.6%	1.8%	0.6%
Uniform elongation (90°)		0.7%	1.5%	1.4%	0.2%
Strain hard. exp.		9.9%	9.3%	1.9%	0.9%
x-position blank		0.3%	0.6%	1.5%	0.5%
y-position blank		0.7%	1.1%	2.6%	1.9%
Unknown		2.1%	2.1%	2.6%	2.6%

variance-based sensitivity analyses are becoming increasingly popular due to their ability to deal with highly complex models since they do not rely on linearity, monotonicity or continuity which allows them to be applied to a wide range of problems [37]. The variance of an input parameter is used as an indicator of importance in terms of fractional contribution to the output variance $V(Y)$. This variance decomposition is often referred to as the Sobol method following [38, 39]. It allows the measurement of main effects of an input parameter by varying X_i alone (first-order sensitivity index S_i) as well as the total effect, which additionally includes all variance caused by its interactions with other parameters (total order sensitivity index S_{Ti}). A solution of multidimensional integrals is required since the computation of the sensitivity indices is based on the decomposition of the function $f(X)$ into summands of increasing dimensionality [39]:

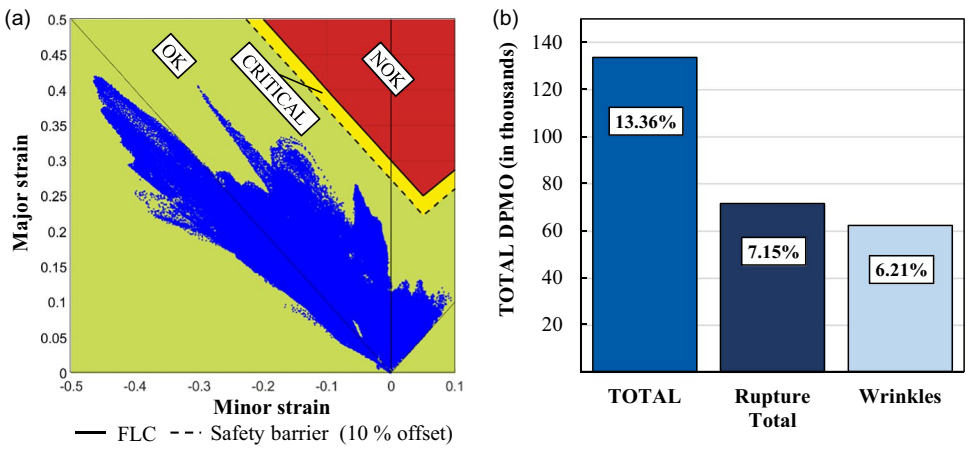

Fig. 7 Classification of the simulation results regarding rupture risk (**a**) and DPMO per quality criterion (**b**)

Table 5 Defects per million opportunities for rupture risk and wrinkling

Quality criteria	abs	%
Necking	65,217	6.52%
Rupture	6,289	0.63%
Wrinkles	62,112	6.21%
Total	133,619	13.36%

$$f(X) = f(X_1, \dots, X_k) = f_0 + \sum_i f_i(X_i) + \sum_i \sum_{j>i} f_{ij}(X_i, X_j) + \dots + f_{1,2,\dots,k}(X_i, \dots, X_k) \quad (2)$$

Thus, in the vast majority of cases, the indices are approximated numerically by the Monte Carlo method using Latin hypercube sampling, pseudo-random or quasi-random numbers. The estimators proposed by Jansen [40] represent best practices in terms of computational costs according to investigations of Saltelli et al. [41] and are applied for the sensitivity analysis in this work. The estimations of the first-order sensitivity index S_i and the total order sensitivity index S_{Ti} according to Jansen are defined as:

$$f_0 \approx \frac{1}{n} \sum_{j=1}^{n} f(\boldsymbol{A})_j \quad (3)$$

$$V(Y) \approx \frac{1}{n} \sum_{j=1}^{n} f^2(\boldsymbol{A})_j - f_0^2 \quad (4)$$

$$S_i \approx \widehat{S}_i = \frac{V(Y) - \frac{1}{2n} \sum_{j=1}^{n} \left(f(\boldsymbol{B})_j - f\left(\boldsymbol{A}_{\boldsymbol{B}}^{(i)}\right)_j \right)^2}{V(Y)} \quad (5)$$

Table 6 Modelling of quality criteria under consideration of different measurand combinations

No	Combination of parameter		Rupture risk	Wrinkling
RSM1	Draw-in	-	86.47%	84.54%
RSM2	Material properties	-	32.04%	32.27%
RSM3	Draw-in	Position blank	86.87%	83.98%
RSM4	Draw-in	Material properties	**92.57%**	**95.06%**
RSM5	Draw-in Blank thickness	Position blank -	83.92%	82.65%
RSM6	Draw-in Blank thickness	Position blank Material properties	86.19%	94.58%
ANN1	Draw-in	-	92.84%	95.33%
ANN2	Material properties	-	57.18%	59.62%

$$S_{Ti} \approx \widehat{S}_{Ti} = \frac{\frac{1}{2n} \sum_{j=1}^{n} \left(f(\boldsymbol{A})_j - f\left(\boldsymbol{A}_{\boldsymbol{B}}^{(i)}\right)_j \right)^2}{V(Y)} \quad (6)$$

The index i runs from one to k representing the number of independent variables, while index j runs from one to n, the number of simulations by the Monte Carlo method. The matrices $\boldsymbol{A}$ and $\boldsymbol{B}$ are two independent sampling matrices with a_{ij} and b_{ij} as generic elements and are generated by a Latin hypercube sampling. The re-sample matrix $\boldsymbol{A}_{\boldsymbol{B}}^{(i)}$ contains all columns from $\boldsymbol{A}$ except the i-th column, which is from $\boldsymbol{B}$. A so-called radial design [42] as recommended in [41] is used to set up $\boldsymbol{A}_{\boldsymbol{B}}^{(i)}$. The design of the re-sample matrix is illustrated in Table 3. The calculations of the sensitivity indices were carried out using the ANN models of the rupture risk and the wrinkling criterion in line with the results of the evaluation of regression models in Table 2.

The Sobol indices are standardized based on the R^2 All, whereas the modelling error and share of influences that cannot be explained by the ANN models are included as 'Unknown' (see Table 4). Both sensitivity indices indicate the friction to be the dominant influence of the process regarding the rupture risk as well as the appearance of wrinkles. However, the material properties appear to affect the process as well, although to a lesser extent. The most influential material property with regard to the rupture risk is the strain hardening exponent, which affects the slope of the flow curve as well as the position of the FLC. Moreover, the sensitivity indices of the rupture risk show that the consideration of interaction effects can lead to a higher influence of the material properties. The higher S_{Ti} of the yield strength and tensile strength compared to their S_i is a result of unfavourable combinations between the tensile and yield strength, which worsen the flow behaviour of the material (high yield strength and low tensile strength). Combinations of low r values may also increase the risk of rupture. An increased influence of material properties on the wrinkling behaviour can only be observed for the r values. Based on the wrinkling criterion ε_{wc} (see Eq. (1)), the wrinkling risk increases with decreasing average anisotropic exponents. The influence of the blank thickness and the position of the blank are not significant and negligible for the application example.

5.2 Evaluation of the process robustness

The results of a sensitivity analysis allow to identify root causes of failure modes and the main influences on the quality criteria, leading to a deeper understanding of the process. However, conclusions about process robustness are not possible, and a process highly dominated by friction, such as the application example in this work, does not

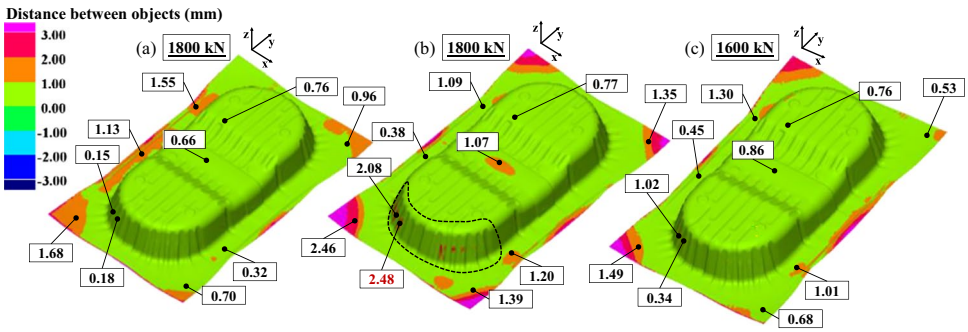

Fig. 8 Comparison of dimensional deviations after 10 parts (part no. 2 with 1800 kN) (**a**), after 350 parts (part no. 3 with 1800 kN) (**b**) and after 460 parts (part no. 5 with 1600 kN) (**c**)

necessarily justify a low robustness. Thus, the evaluation of the process robustness and performance is necessary. It can be realized by the calculation of the DPMO, which has the advantage of considering multiple defects of the same type and does not rely on an upper and lower specification limit such as the Cpk value. Therefore, the DMPO is a suitable criterion to assess robustness based on the rupture risk and wrinkling, since both criteria rely on an upper limit only. One possibility to identify challenging processes based on DPMO is the evaluation of shift reports from series production. However, results from variant simulations can be a good alternative if a reliable data basis from series production is lacking. In this work, the simulation results are classified into three different categories in terms of rupture risk (Fig. 7a). Simulations containing nodes above the FLC are considered failed parts (NOK) and simulations with all nodes below the safety barrier as good parts (OK), and the remaining results are classified as critical. The offset of 10% to the FLC which defines the critical area is derived from internal guidelines and represents parts, where necking can be expected, while wrinkles are observed for values above 0.25. The total DMPO for both quality criteria is summarized in Fig. 7b, while Table 5 shows all DPMO values. Processes with expected scrap rates above 5% are considered difficult with low robustness.

This applies both to the application example in terms of rupture risk and to the occurrence of wrinkles justifying the implementation of an operator assistance system. It has to be considered that the appearance of ruptured parts is predicted to be comparably unlikely, which is in fact in line with the experience from series production. In general, parts are already rejected, and process parameters are adjusted as soon as necking is detected. Furthermore, the large number of parts in the critical area of necking indicates close operation at the process limits.

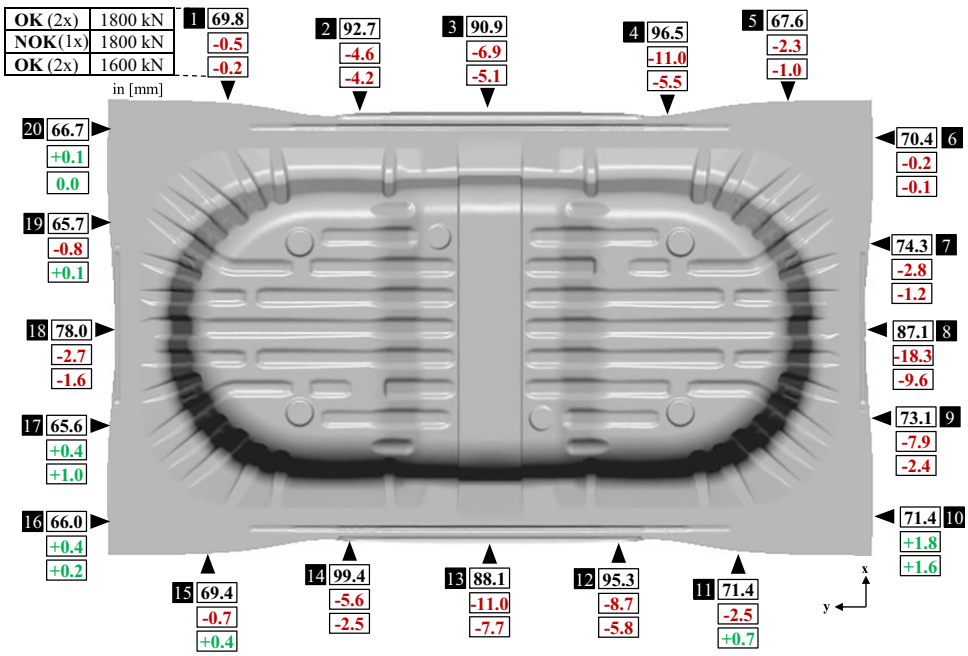

Fig. 9 Influence of the blank holder force on the material flow

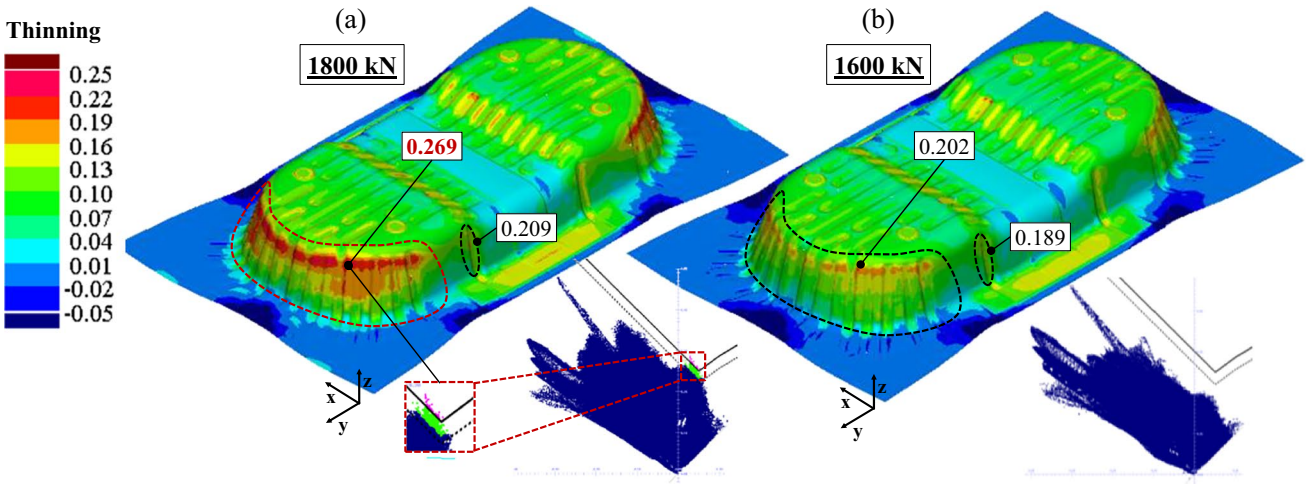

Fig. 10 Comparison of thinning and rupture risk at homogeneous initial tool temperatures of 60 °C and 1800 kN (**a**) and 1600 kN (**b**) blank holder force under consideration of the nominal parameter set

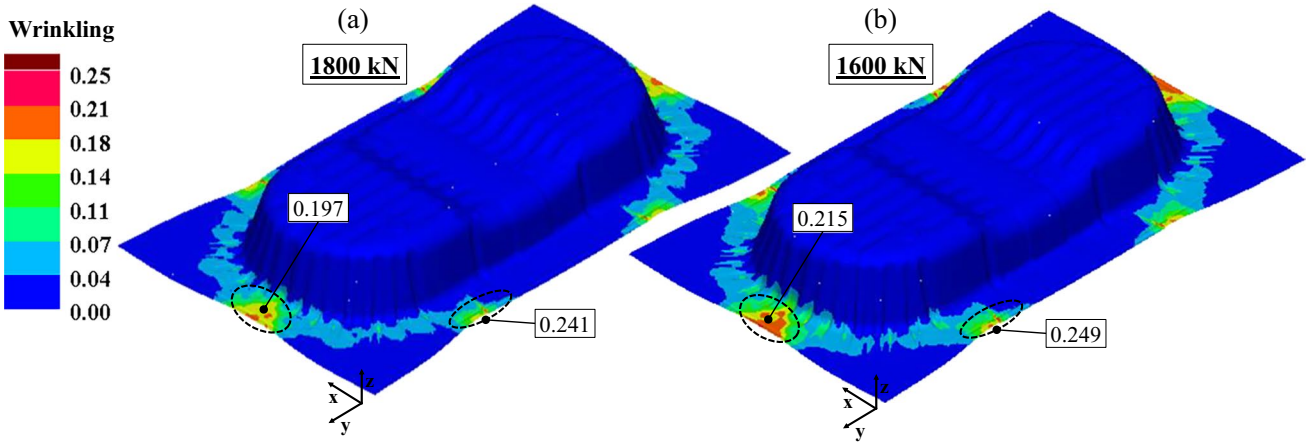

Fig. 11 Comparison of wrinkling at homogeneous initial tool temperatures of 60 °C and 1800 kN (**a**) and 1600 kN (**b**) blank holder force under consideration of the nominal parameter set

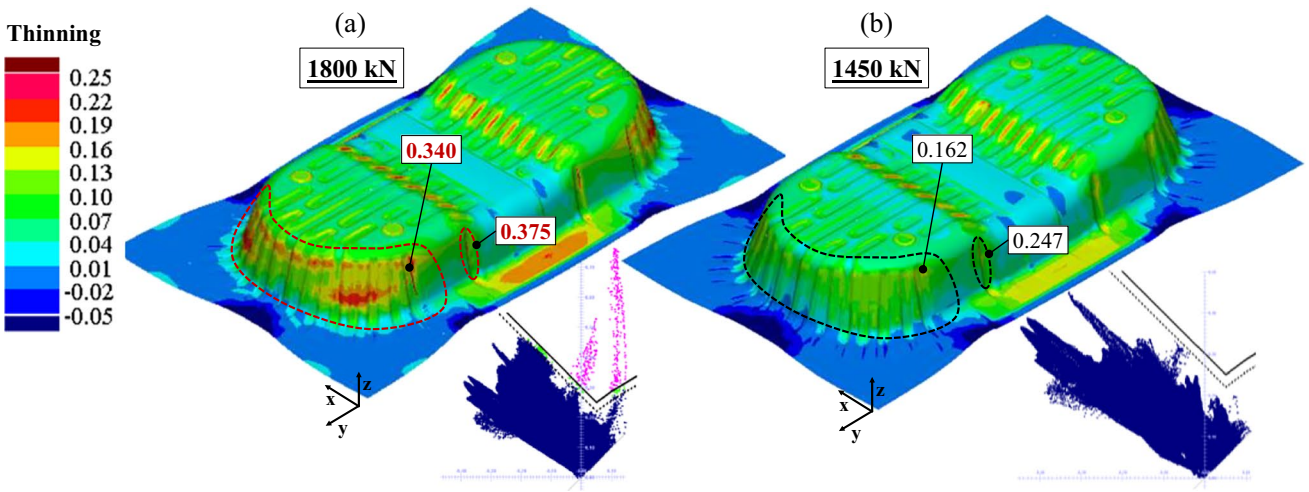

Fig. 12 Comparison of thinning and rupture risk at homogeneous initial tool temperatures of 60 °C and 1800 kN (**a**) and 1450 kN (**b**) blank holder force under consideration of the worst-case parameter set

Table 7 Unfavourable parameters with regard to rupture risk

Parameter	Value
Friction coefficient	$\mu_G(p, v_{rel}, T)$
Blank thickness	0.6615 mm
Yield strength	217 MPa
Tensile strength (0°/45°/90°)	326/339/321 MPa
r value (0°/45°/90°)	1.91/1.28/2.17
Uniform elongation (0°/45°/90°)	20.3/17.1/19.7%
Strain hard. exp	0.186
x-position blank	+0.04 mm
y-position blank	−1.11 mm

5.3 Preselection of measurands based on observability

In most cases, it is difficult to draw conclusions regarding the part quality during the forming process since quality criteria and failure modes are not directly measurable. A measurement after the forming process is usually associated with a high effort, leading to a significant loss in productivity if a broad sample is to be taken into account. Thus, observers are often utilized to provide an estimate of the part quality. The quality criteria rupture risk and wrinkling are approximated based on different combinations of measurable input parameters using the RSM as before, i.e. either a MLR or MQR model is used. However, the friction coefficient is omitted as input to the models due to the lack of measurement possibilities and the flange draw-in serves as possible input instead. The observability per combination is quantified by the achievable R^2 after cross-validation (Table 6). In a first step, a combination set considering all input parameters is used (combination set no. RSM6). A stepwise regression based on the backward elimination approach is carried out to determine the optimal combination of measurands per quality criterion. Thus, only parameters with an added value to the goodness-of-fit will be left in that model. Not all draw-in positions or material parameters are necessarily included as consequence of this approach. The results of these ideal combinations per quality criterion are highlighted by underlining in Table 6. The observability analysis indicates a combination of draw-in, and material properties (no. RSM4) appear to be the most promising solution in terms of the achieved R^2.

However, the measurement of the draw-in is essential to draw conclusions regarding the rupture risk and the appearance of wrinkles. The consideration of the measurement of material properties only provides a small advantage. Especially a sole measurement of material properties (no. RSM2) is not recommended since it does not allow a reliable and trustworthy statement about the selected quality criteria due to the low R^2. The same applies to the blank thickness and the position of the blank. The consideration of the blank position at the beginning of the process leads to a slight increase of the observability at least for the rupture risk, while both together may even reduce the observability of the process, as shown by combination no. RSM5 and no. RSM6. This is in agreement with the results of the sensitivity analysis regarding the dominant influence of friction, taking into account that the draw-in is a suitable indicator to reflect changes of the frictional behaviour due to changes in the resulting restraining forces [43]. The application of a more complex model like ANN allows the reduction of the number of necessary measurands without loss in performance (no. ANN1) compared to the ideal set or at least enables an increase in observability (no. ANN2).

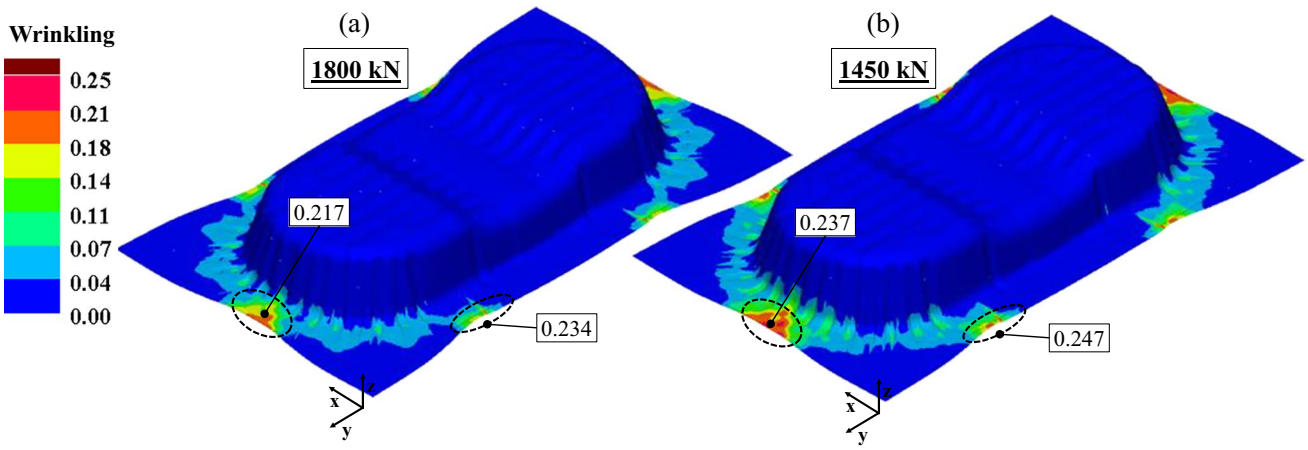

Fig. 13 Comparison of wrinkling at homogeneous initial tool temperatures of 60 °C and 1800 kN (**a**) and 1450 kN (**b**) blank holder force under consideration of the worst-case parameter set

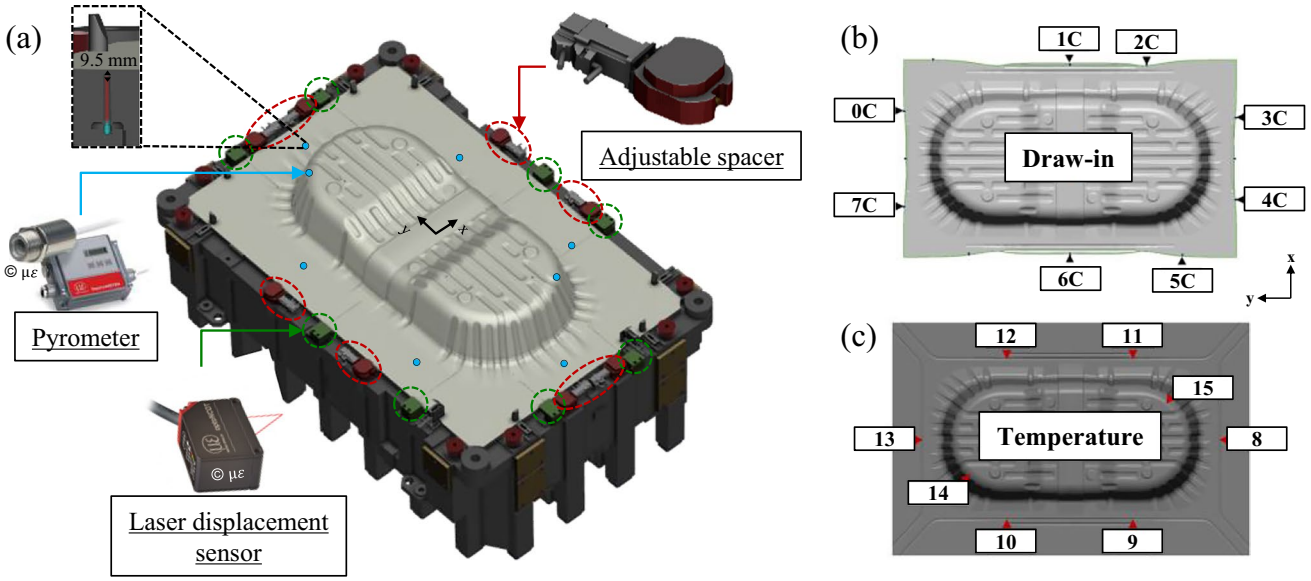

Fig. 14 Sensor technology implemented in the blank holder including adjustable spacers (**a**), measuring positions of the draw-ins (**b**) and measuring positions of the tool temperatures (**c**)

5.4 Controllability and compensation strategy

In the series production of car body parts, there is usually a limited number of actuators available for process intervention. All measures have in common that an adjustment of the material flow within the process is aimed when quality issues or part failures arise. Adjustments of the blank holder force or the height of the spacers leading to different global or local pressure conditions can compensate part failure due to adapted restraining forces. Furthermore, it is possible to increase the amount of lubrication of the blanks to enable a greater material flow. However, the effectiveness of these measures has to be analysed to evaluate the controllability of the process and to derive possible compensation strategies. In this work, the adjustment of the blank holder force is used to analyse whether the process is generally controllable. For this purpose, a sample of five deep drawn parts was taken from a production run at different times and digitized by a GOM Atos system. Two parts were taken at the beginning of the production and do not include any part failure. The third part was taken after necking in the right rib was detected forcing the machine operator to reduce the blank holder force uniformly from 1800 to 1600 kN. The two remaining parts were taken after adjusting the blank holder force and meet the quality requirements. A comparison of the dimensional deviations between the second, the third and the last part using the first part as reference is shown in Fig. 8. For this part, only a low variability of dimensional deviations is observed during the production run. Furthermore, the dimensional deviations between the first and the third digitized part reveal the necking in the right rib of the third part (Fig. 8b). This deviation in the rib of the part vanishes almost completely after the reduction of the blank holder force, Fig. 8c shows.

These observations are consistent with measurement results regarding the flange draw-in of the parts. A comparison with regard to the flange draw-in of all parts is shown in Fig. 9. The draw-in positions correspond to Fig. 5. A decrease of the flange draw-in in almost the whole part can be observed until necking is detected. However, the change in flange draw-in is not uniform as would be expected from a symmetrical component in an idealized case. The decrease of the flange draw-in on the right side (pos. 6–10) is significantly higher than on the left side (pos. 16–20) and leads to necking. Differences can also be observed between positions 3 and 13.

In agreement with the results of the sensitivity analysis, an increased friction coefficient due to the heating of the tools leads to higher restraining forces and thus to failure of the part. However, the reduction of the blank holder force allows an increase of the material flow leading to an improved thinning behaviour. Faultless parts are regained although the draw-in reaches the initial state at individual positions only. The possibility of compensating for such formability issues by a simple reduction of the blank holder force can also be confirmed by simulation results. For this purpose, an advanced thermal–mechanical coupled simulation is used, taking into account a friction model that depends on the sliding velocity, contact pressure and temperature. Detailed information on the mechanical and thermal properties as well as the contact and friction modelling

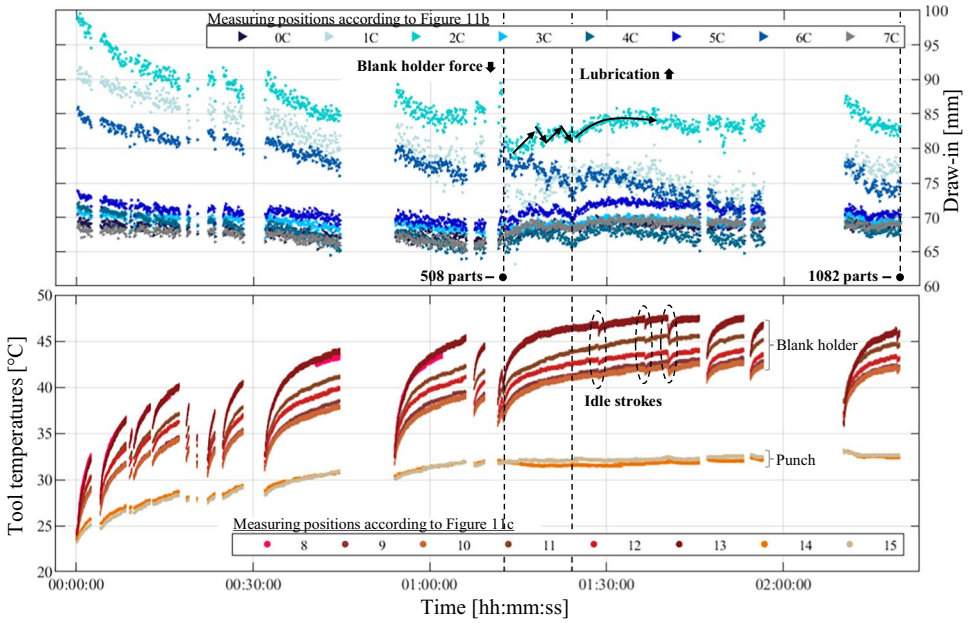

Fig. 15 Measurement of the draw-in and the tool temperatures in series production [43]

of this simulation can be found in [44]. Assuming a simplified initial homogeneous temperature on the tools of 60 °C and an initial metal sheet temperature of 20 °C, rupture and necking are to be expected in the rib of the part (see Fig. 10a). A reduction of the blank holder force as is done in series production results in decreased restraining forces and an improved formability in terms of thinning without rupture or necking. However, reducing the blank holder force may facilitate the formation of wrinkles, especially in the flange of the part. Severe wrinkling was not observed in any of the parts from the production sample. According to the simulation results, the reduction of the blank holder force causes only a slight increase in wrinkling, which is not significant and negligible (see Fig. 11). It can be expected that a reduction of the blank holder force is a sufficient compensation option in the vast majority of cases, since friction is the most influential parameter of the process with regard to the appearance of rupture and wrinkles.

However, the simulation results from Figs. 10 and 11 are based on the nominal values (see Table 1) and neglect further negative influences on the formability of the part which are caused by other parameters, especially by varying material properties. For this purpose, the metamodels are used to determine the most unfavourable parameter set in terms of rupture based on a sampling matrix with 10,000 parameter sets generated by Latin hypercube sampling, considering a constant friction coefficient and the variation ranges from Table 5. The unfavourable parameters of this scenario can be found in Table 7.

In this worst-case scenario, rupture and necking in the rib of the part are expected at initial homogeneous tool temperatures of 60 °C as before (see Fig. 12a). However, the thinning and risk of rupture are considerably higher. Reducing the blank holder force is still an effective way of improving formability in terms of excessive thinning. In contrast to the first case, a lower blank holder force is

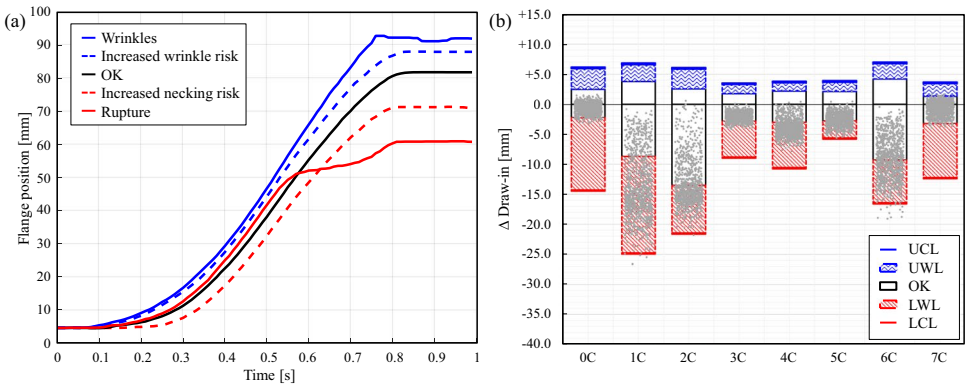

Fig. 16 Characteristic draw-in curves (position 6C) (**a**) and upper and lower limits of the flange draw-in regarding main failure criteria (**b**)

necessary to compensate for the negative effects. Although an increased risk of wrinkles can be observed, it is still not significant (see Fig. 13).

6 Selection of sensor technologies and implementation of an assistance system

The results of the process analysis have shown that the implementation of an operator assistance system is expedient and justifiable for the application example. The consideration of the flange draw-in as sole measurand is the most reliable and efficient solution based on the results of the observability analysis and is supported by the investigation of the process controllability. However, the specific selection of sensor technologies to measure the draw-in is difficult. A generally valid quantitative and objective evaluation of existing solutions is practically impossible since most draw-in measurement solutions are in-house developments which are not available on the market such as a sheet metal tongue [10], a track ball [6], an eddy current sensor [45], image sensor technologies [46] or camera-based systems [14, 17]. Thus, this step is strongly specific, depending on economic factors and development resources as well as the basic circumstances in the press shop and the press line. All solutions are tool-integrated and spot measurement systems, except for camera-based systems, which allow a measurement of the draw-in outline independent of the process if integrated into the press line. However, the costs regarding hardware, development, implementation and calibration are comparatively high. Furthermore, the draw-in curve and varying positions of the sheet metal are neglected. A measurement system based on laser triangulation sensors is the most appropriate solution in most cases due to the high benefits in terms of an economic point of view. Numerous types of laser triangulation sensors are available on the market and usually ensure a plug-and-play principle for fast installation and commissioning. The biggest disadvantage is the restriction regarding positioning possibilities due to drawbeads or step beads in the tools. An accurate and complete measurement of the draw-in can only be performed up to the drawbead in this case. The determination of appropriate measurement positions is strongly recommended before installation, even if the repositioning effort is comparatively low.

For the purpose of this work, a measurement system based on laser triangulation sensors was integrated into the drawing tools of the application example (Fig. 14a). The flange draw-in is recorded inline at eight different positions by laser displacement sensors of the type optoNCDT 1420 from Micro-Epsilon. The risk of contamination by dirt is reduced to a minimum by using a casing. The exact positions as shown in Fig. 11b have been derived from the results of

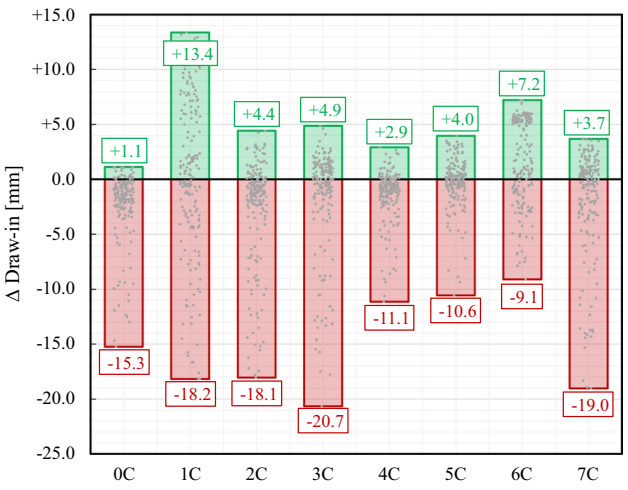

Fig. 17 Achievable draw-in differences by the spacers under consideration of a constant blank holder force and no additional lubrication

Fig. 9. All 20 positions have been ranked according to their draw-in variability due to the heating of the tools (draw-in deviation between OK parts and NOK part at 1800 kN) and their draw-in variability after the reduction of the global blank holder force (draw-in deviation between NOK part at 1800 kN and OK parts at 1600 kN).

The positions 8, 12 and 14 have not been selected due to restrictions caused by the drawbeads, although they show a high variability. The low draw-in variability on the left side of the part (positions 16–20) does not justify placing a draw-in sensor there. However, the tools were also equipped with adjustable spacers controlling their heights by servomotors to manipulate local pressure conditions and thus the local material flow, as described in [17]. The electrically driven spacers replaced eight of a total of sixteen conventional spacers, including two spacers on the left side. Therefore, two laser displacement sensors were installed on the left side of the blank holder to monitor the material flow at these positions as well. Temperature changes of the tools are recorded by eight pyrometers on the backside of the blank holder and punch. The integration of Micro-Epsilon's CT-SF15-C3 pyrometers into drill holes reaching 9.5 mm to the tool surface allows a convenient configuration due to the creation of a black body. The measured temperatures at the bottom of the holes can be assumed as approximately equal to the surface temperatures. The six pyrometers in the blank holder (8–13) are arranged symmetrically and point to the drawbead, whereas sensors 14 and 15 measure the temperature of the punch radius (Fig. 14c). Their consideration is only of secondary importance and is not decisive for the application of the operator assistance system. Nevertheless, sensor information about the development of the tool temperature during the process provides insight into frictional changes. The contact pressure and sliding velocity as one of

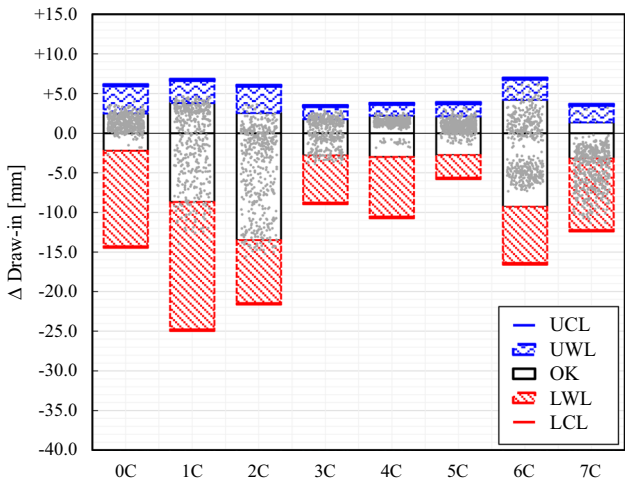

Fig. 18 Controlled production run for a batch size of 497 parts

the main influences on friction in sheet metal forming [47] can be assumed to be approximately constant in series production if manipulating variables such as the blank holder force or the stroke rate are not adjusted or varied. As a consequence, temperature-induced friction effects are expected to be substantial for friction-dominated processes.

6.1 Identification of the component state

A process monitoring system is set up based on the presented measurement system. Information regarding the draw-in and the tool temperatures is monitored throughout the process, and the occurrence of potential part failures is submitted to the machine operator via warning message. Such a monitoring system corresponds to a second-level assistance system according to [48] and offers the possibility to increase the transparency of the manufacturing process. Statistical process control (SPC) [49] based on the draw-in per sensor is used for process monitoring purposes and the identification of the component state with respect to the main failure criteria of necking and rupture

Table 8 Distribution of drawn parts per SPC limit of an uncontrolled and controlled production run

SPC limits	*Uncontrolled*		*Controlled*	
	abs	*%*	*abs*	*%*
UCL	0	0.00%	0	0.00%
UWL	1	0.08%	36	7.23%
OK	640	59.14%	412	82.86%
LWL	437	40.57%	49	9.91%
LCL	4	0.21%	0	0.00%
TOTAL	1082	100%	497	100%

as well as wrinkling. The machine operator was informed as soon as a measurement position leaves the predefined range of faultless parts. The determination of the warning and control limits per sensor position requires information about their reference values and the corresponding variation range in which faultless parts are produced. For this purpose, measurement data from series production, consisting of 12,234 parts from a total of 32 production runs, were evaluated. The reference values represent the average value of the draw-in from the first 10 parts of each production run as long as no significant change in tool temperature was observed ($\Delta T_{tools} \leq 1°C$). The distance from the reference value to the upper and lower limits is largest. In general, an increasing draw-in increases the risk of wrinkles, whereas a decreased draw-in may trigger necking and rupture. The control limits (CL) at which necking and rupture or wrinkles are to be expected were also derived from the production data. The development of the draw-in and the tool temperatures for an exemplary production run with a batch size of 1082 deep drawn parts and a stroke rate of 11 strokes per minute is shown in Fig. 15. Each triangle represents the draw-in of a drawn part including the corresponding tool temperatures. The measurement system only records data when the press is running to keep the data volume as small as possible. Gaps in the figure thus indicate breaks and interruptions during production.

The measurement data will not be discussed in-depth in this paper, since a detailed analysis with regard to the influence of temperature, blank holder force and lubrication on the material flow in the flange has already been carried out in [43].

In brief, it was found that the material flow of the process is mainly driven and disturbed by the tool temperature, resulting in higher friction and increased restraining forces, which lead to a decreased draw-in and cause part failure due to necking and tearing. As a consequence, the cylinder pressure in the drawing cushion was reduced after 508 parts by the machine operator in order to stabilize the process. The draw-in per sensor position at that time is used as the lower control limit (LCL) with respect to the occurrence of necking and rupture. All production runs are evaluated according to this procedure, enabling the determination and refinement of the CL values regarding necking, rupture and wrinkles. Fig. 16a shows the corresponding draw-in curves exemplarily for sensor position 6C according to the measurement positions from Fig. 14b. The draw-in curve representing necking shows a similar shape compared to the reference curve, except for the final draw-in. However, the shape changes as soon as rupture occurs. The final draw-in is not only significantly lower, but the material flow decelerates abruptly and almost stops after 0.55 s, since critical tensile stresses in the rib of the part exceed the tensile strength of

the material and lead to rupture. The material flow in the flange does not stop completely because the final drawing depth has not yet been reached. However, the deceleration of the material flow indicates that the rupture acts like a relief cut supporting the material flow in the rib; thus, the material has not primarily to come from the forming zone in the flange. The resulting lower and upper control limits (UCL) and warning limits (WL) per sensor position regarding the main failure criteria after evaluation of all production runs are shown in Fig. 16b. Since the process is highly dominated by temperature-induced friction effects leading to excessive thinning, the occurrence of wrinkles is comparatively less frequent, resulting in a smaller data basis of parts with wrinkles. The lower and upper limits as well as the area of faultless parts indicate that the sensor positons 1C, 2C and 6C are the most sensitive with respect to the process. Since the assistance system is intended to support the machine operator even before part failure occurs, warning limits have been specified to represent areas of increased risk in terms of necking and wrinkles. Twenty percent of the total data above the LCL defines the lower warning limit (LWL) and thus the area of increased necking risk, whereas 20% of the total data below the UCL represents the upper warning limit (UWL) and an increased risk of wrinkling. This assumption was made due to the lack of thinning and wrinkling data of each part and does not necessarily imply the occurrence of part failure. A complete measurement of each part with regard to thinning and wrinkling after the forming process is basically not possible in series production. However, consistent avoidance of this area will improve the overall quality of the production batch by drawing as few parts as possible close to these limits. The draw-in differences between the reference values and the actual values per sensor position (Δ Draw-in) of the exemplary production run from Fig. 15 are included in Fig. 16b. Each point represents a drawn part. It can be observed that a large number of parts were produced below the LWL and close to the process limits most likely, although they appeared unremarkable in production.

6.2 Decision-making assistance for the operator

A fourth-level assistance system does not only present information regarding the transition of the process from a permissible to an impermissible state, but also provides the machine operator with a suitable action recommendation based on real-time data [48]. In the present work, a decision-making assistance is provided as soon as a warning limit is exceeded; otherwise, the default parameters of the process are recommended. The assistance is based on a model using experimental results under consideration of varying manipulated variables. The DoE is generated by a Latin hypercube sampling, which accounts for the variation in height of eight adjustable spacers within the range of ± 0.34 mm to manipulate local pressure conditions and the local material flow. A uniform distribution considering no correlations was used for the calculation of the DoE, in contrast to the parameters of the variant simulations, which are based on normal distributions under consideration of correlations between the material parameters. The experiments were carried out at room temperature, and a variation of the blank holder force as well as the lubrication amount was not considered. Furthermore, the experimental procedure is extended to include the variation of single spacer positions as well as the simultaneous variation of all spacers, resulting in a total of 191 experiments and deep drawn parts. The maximum achievable draw-in deviations to the references values (Δ Draw-in) per sensor position are shown in Fig. 17. As before, each point represents a drawn part. The values cannot be combined arbitrarily and show extreme values, i.e. reaching a maximum draw-in deviation can also have an influence on the draw-in at other sensor positions. The data indicates that it is generally possible to control the process only by adjusting the height of the spacers. Both wrinkles and necking and rupture can be adequately prevented, leading to an increased distance of the actual draw-in to the warning and control limits if appropriate spacer heights are applied. However, the relationship between the spacer heights and the resulting draw-in deviations is non-linear and requires complex models due to the multiple input and multiple output. Multivariate multiple regression models only provide very poor results regarding the goodness-of-fit. The same applies for ANN models, although this is likely due to the comparatively small amount of experimental data. Thus, recommendations based on these models would be associated with a very high degree of uncertainty. Nevertheless, in order to be able to provide the machine operator with a decision-making assistance and a suitable configuration of the spacer heights during the process as soon as the warning limit is exceeded, a 1-nearest-neighbour classifier is applied.

This classifier is a special case of the k-nearest-neighbour and does not require learning, since it assigns a point to its closest neighbour in feature space among training points based on a predefined distance metric.

In the present case, the measured draw-in deviations are assigned to the closest neighbour from the experimental database during the process, with the aim of minimizing the Δ Draw-in of the next part at every position. The operator receives a recommendation for a suitable adjustment of the spacers after each stroke. This approach can be considered off-line control [5] and assumes that the process conditions do not change suddenly between two consecutive parts, since the recommended settings of the current part are based on the draw-in measurements of the previous part. The determination of the distance enabling this classification uses the standardized Euclidian distance between two J-dimensional vectors as proposed by Slater [50]:

$$d_{st} = \sqrt{\sum_{j=1}^{J} \frac{\left(x_{sj} - y_{tj}\right)^2}{s_j^2}} \tag{7}$$

where x_{sj} is the actual Δ Draw-in, y_{tj} is the Δ Draw-in from the experimental database and s_j is the standard deviation of the j-th variable or sensor position. Standardization avoids that values with large intersample differences dominate the calculation suppressing individual sensor positions. This is the case for positions 1C, 2C and 6C which show the highest variation in the process.

6.3 Proof of concept trial

The operator assistance system, consisting of the process monitoring and the decision support, was transferred into a human machine interface (HMI) based on National Instruments' LabVIEW for the visual interface and MathWorks' MATLAB for the calculations. A simplified software-in-the-loop simulation using raw data from past productions runs was generated as an ideal test environment for debugging purposes, before testing the operator assistance system under real production conditions. After successful troubleshooting, a proof of concept trial was carried out in series production considering a batch size of 497 parts and a stroke rate of 11 strokes per minute. The draw-in differences between the reference values and the actual values per sensor position (Δ Draw-in) of this controlled production run are included in Fig. 18.

As before, each point represents a drawn part. The heights of the spacers were adjusted a total of four times based on the recommendation of the operator assistance system after the draw-in has exceeded the LWL. All parts meet the quality requirements, and there was no scrap produced due to early intervention. A clear shift of the draw-ins to their reference values can be observed in comparison to the results of the exemplary production run from Fig. 16b, except for the draw-in of sensor position 7C. However, a majority of the parts has been produced within their warning limits. The average number of parts per sensor position within their warning limits (OK area), outside their warning limits (UWL and LWL area) and outside their control limits for the uncontrolled and controlled production run can be found in Table 8. The distribution of parts confirms that the number of parts within the LWL has been significantly reduced resulting in a greater proportion of parts within their warning limits. As a result, the overall quality of the parts produced was improved by the operator assistance system.

7 Conclusion and outlook

The approach for a development of an operator assistance system as proposed in this work serves as a guideline to fulfil the need for a more robust process. A thorough process analysis using variant simulations offers a cost-efficient evaluation regarding the expediency of an operator assistance system and the identification of suitable and mandatory sensor technologies to ensure a successful implementation. Processes which do not justify an operator assistance system can be detected at an early stage avoiding unnecessary expenses. The process of the application example introduced in this work justified the implementation of an assistance system based on draw-in measurements. The variance-based sensitivity analysis predicted a strong influence of friction on both quality criteria rupture risk and wrinkling, which was confirmed by measurements from series production. Furthermore, it could be shown that the process is controllable through typical manipulated variables such as the blank holder force and the lubrication amount as well as the adjustment of the spacer heights. An operator assistance system consisting of SPC-based process monitoring and a decision-making assistance using a 1-nearest-neighbour algorithm considering varying spacer heights only is a promising strategy to significantly stabilize and improve the process. A proof of concept trial in series production showed that the operator assistance system is capable of significantly improving the overall quality of the parts produced. Nonetheless, it is expected that the actuating limits of the decision-making assistance caused by the focus on adjustable spacers can be extended by the varying of the blank holder force and, if necessary, additional lubrication amounts.

Acknowledgements This research was carried out within the project 'ASPECT – Advanced Simulation and control of tribology in metal forming Processes for the North-West European Consumer goods and Transport sectors', co-funded by the INTERREG North West Europe programme, www.nweurope.eu/aspect. The authors wish to thank for funding the project. The project partner ESI GmbH is also gratefully acknowledged for their support.

Author contribution Not applicable.

Funding Open Access funding enabled and organized by Projekt DEAL. The research was co-funded by the INTERREG North West Europe programme www.nweurope.eu/aspect.

Data availability Data and material are not available due to legal and commercial restrictions.

Code availability Data and material are not available due to legal and commercial restrictions.

Declarations

Ethics approval Not applicable.

Content to participate Not applicable.

Content to publication Not applicable.

Conflict of interest The authors declare no competing interests.

References

1. Hirsch J (2011) Aluminium in innovative light-weight car design. Mater Trans 52:818–824. https://doi.org/10.2320/matertrans.L-MZ201132
2. Cischino E, Di Paolo F, Mangino E et al (2016) An advanced technological lightweighted solution for a body in white. Transportation Research Procedia 14:1021–1030. https://doi.org/10.1016/j.trpro.2016.05.082
3. Cheah LW (2010) Cars on a Diet: The Material and Energy Impacts of Passenger Vehicle Weight Reduction in the US. Doctoral dissertation, Massachusetts Institute of Technology
4. Hortig D (2011) Experiences with the robustness of sheet metal forming processes. Proc. FTF 2011
5. Allwood JM, Duncan SR, Cao J et al (2016) Closed-loop control of product properties in metal forming. CIRP Ann 65:573–596. https://doi.org/10.1016/j.cirp.2016.06.002
6. Griesbach B (2000) In-Prozeß Stoffflußmessung zur Analyse und Führung von Tiefziehvorgängen. Doctoral dissertation, Universität Hannover. Berichte aus dem Institut für Umformtechnik und Umformmaschinen, vol 547
7. Sturm V (2013) Einfluss von Chargenschwankungen auf die Verarbeitungsgrenzen von Stahlwerkstoffen. Doctoral dissertation, Universität Erlangen-Nürnberg
8. Purr S, Wendt A, Meinhardt J et al (2016) Data-driven inline optimization of the manufacturing process of car body parts. IOP Conference Series Materials Science and Engineering 159:12002. https://doi.org/10.1088/1757-899X/159/1/012002
9. Faaß I (2009) Prozessregelung für die Fertigung von Karosserieteilen in Presswerken. Doctoral dissertation, Technische Universität München
10. Straube O (1994) Untersuchungen zum Aufbau einer Prozeßregelung für das Ziehen von Karosserieteilen. Doctoral dissertation, Technische Universität Berlin
11. Fenn RC (1989) Closed-loop control of forming stability during metal stamping reduction in the US. Doctoral dissertation, Massachusetts Institute of Technology
12. Hardt DE, Fenn RC (1993) Real-time control of sheet stability during forming. Journal of Engineering for Industry 115:299–308. https://doi.org/10.1115/1.2901664
13. Bräunlich H, Neugebauer R (2001) Closed loop control of deep drawing processes. SheMet 2001:529–538
14. Neumann A, Hortig D, Merklein M (2011) Measurement of material flow in series production. KEM 473:137–144. https://doi.org/10.4028/www.scientific.net/KEM.473.137
15. Maier S, Schmerbeck T, Liebig A et al (2017) Potentials for the use of tool-integrated in-line data acquisition systems in press shops. J Phys: Conf Ser 896:12033. https://doi.org/10.1088/1742-6596/896/1/012033
16. Hansen B, Purr S, Meinhardt J et al (2019) Investigation of the tribological behavior of car body parts in series production. Procedia Manufacturing 27:51–56. https://doi.org/10.1016/j.promfg.2018.12.043
17. Kraft M, Bürgel U (2017) Novel concept for measurement of global blank draw-in when deep drawing outer skin automotive components. J Phys: Conf Ser 896:12034. https://doi.org/10.1088/1742-6596/896/1/012034
18. Fischer P, Heingärtner J, Aichholzer W et al (2017) Feedback control in deep drawing based on experimental datasets. J Phys: Conf Ser 896:12035. https://doi.org/10.1088/1742-6596/896/1/012035
19. Barthau M, Liewald M (2017) New approach on controlling strain distribution manufactured in sheet metal components during deep drawing process. Procedia Engineering 207:66–71. https://doi.org/10.1016/j.proeng.2017.10.740
20. Fischer P, Heingärtner J, Duncan S et al (2020) On part-to-part feedback optimal control in deep drawing. J Manuf Process 50:403–411. https://doi.org/10.1016/j.jmapro.2019.10.019
21. Hoffmann H Zäh MF Faass I et al (2007) Automatic process control in press shops. KEM 344:881–888. https://doi.org/10.4028/www.scientific.net/KEM.344.881
22. Gräler M, Springer R, Henke C et al (2018) Assisted setup of forming processes: compensation of initial stochastic disturbances. Procedia Manufacturing 25:358–364. https://doi.org/10.1016/j.promfg.2018.06.104
23. Traub T, Gregório MG, Groche P (2018) A framework illustrating decision-making in operator assistance systems and its application to a roll forming process. Int J Adv Manuf Technol 97:3701–3710. https://doi.org/10.1007/s00170-018-2229-x
24. Hora P, Heingärtner J, Manopulo N et al (2011) On the way from an ideal virtual process to the modelling of the real stochastic. Proc. FTF 2011
25. Swift HW (1952) Plastic instability under plane stress. J Mech Phys Solids 1:1–18. https://doi.org/10.1016/0022-5096(52)90002-1
26. Abspoel M, Scholting ME, Lansbergen M et al (2017) A new method for predicting advanced yield criteria input parameters from mechanical properties. J Mater Process Technol 248:161–177. https://doi.org/10.1016/j.jmatprotec.2017.05.006
27. Abspoel M, Scholting ME, Lansbergen M et al (2017) Accurate anisotropic material modelling using only tensile tests for hot and cold forming. J Phys: Conf Ser 896:12049. https://doi.org/10.1088/1742-6596/896/1/012049
28. DIN EN ISO 12004-2:2021-07 Metallic materials - Determination of forming-limit curves for sheet and strip - Part 2: Determination of forming-limit curves in the laboratory (ISO 12004-2:2021)
29. Goodwin GM (1968) Application of strain analysis to sheet metal forming problems in the press shop. In: SAE Technical Paper Series. SAE International400 Commonwealth Drive, Warrendale PA
30. Keeler SP (1961) Plastic instability and fracture in sheets stretched over rigid punches. Doctoral dissertation, Massachusetts Institute of Technology
31. Harsch D, Heingärtner J, Hortig D et al. (2017) Observability of quality features of sheet metal parts based on metamodels.

COMPLAS XIV: proceedings of the XIV International Conference on Computational Plasticity: fundamentals and applications, 692–703
32. Emrich A, Liewald M, Ruf G (2011) Stochastic analysis in FE-simulation of sheet metal forming as a key enabler for a robust production process. Proc. FTF 2011
33. Bonte MHA (2007) Optimisation strategies for metal forming processes. Doctoral dissertation, University of Twente
34. Harsch D, Heingärtner J, Renkci Y et al. (2017) Influence of scattering material properties on the robustness of deep drawing processes. Proc. FTF 2017
35. AutoForm Engineering GmbH (2017) AutoForm R7.0.2 Software Manual. AutoForm Engineering GmbH
36. Marquardt DW (1963) An algorithm for least-squares estimation of nonlinear parameters. J Soc Ind Appl Math 11:431–441. https://doi.org/10.1137/0111030
37. Iooss B, Lemaître P (2015) A review on global sensitivity analysis methods. In: Dellino G, Meloni C (eds) Uncertainty Management in Simulation-Optimization of Complex Systems: Algorithms and Applications. Springer, US, Boston, MA, pp 101–122
38. Sobol' IM (2001) Global sensitivity indices for nonlinear mathematical models and their Monte Carlo estimates. Math Comput Simul 55:271–280. https://doi.org/10.1016/S0378-4754(00)00270-6
39. Sobol' IM (1993) Sensitivity analysis for non-linear mathematical models. Mathematical modelling and computational experiment 4:407–414
40. Jansen MJ (1999) Analysis of variance designs for model output. Comput Phys Commun 117:35–43. https://doi.org/10.1016/S0010-4655(98)00154-4
41. Saltelli A, Annoni P, Azzini I et al (2010) Variance based sensitivity analysis of model output. Design and estimator for the total sensitivity index. Comput Phys Commun 181:259–270. https://doi.org/10.1016/j.cpc.2009.09.018
42. Saltelli A (2002) Making best use of model evaluations to compute sensitivity indices. Comput Phys Commun 145:280–297. https://doi.org/10.1016/S0010-4655(02)00280-1
43. Kott M, Erz C, Heingärtner J et al (2020) Controllability of temperature induced friction effects during deep drawing of car body parts with high drawing depths in series production. Procedia Manufacturing 47:553–560. https://doi.org/10.1016/j.promfg.2020.04.166
44. Krairi A, Marmi J, Gastebois S et al (2020) A speed-up method for numerical simulations of multi-strokes cold metallic sheet forming processes. Procedia Manufacturing 47:570–577. https://doi.org/10.1016/j.promfg.2020.04.173
45. Forstmann U, (2000) Induktive Wegsensoren zur Überwachung und Regelung des Blecheinzugs beim Tiefziehen. Zugl.: Berlin, Techn. Univ., Diss., (2000) Berichte aus dem Produktionstechnischen Zentrum Berlin. IPK Fraunhofer Institut Produktionsanlagen und Konstruktionstechnik, Berlin
46. Doege E, Seidel H-J, Griesbach B et al (2002) Contactless on-line measurement of material flow for closed loop control of deep drawing. J Mater Process Technol 130–131:95–99. https://doi.org/10.1016/S0924-0136(02)00763-X
47. Oden JT, Martins JA (1985) Models and computational methods for dynamic friction phenomena. Comput Methods Appl Mech Eng 52:527–634
48. Klocke F, Kamps S, Mattfeld P, Shirobokov A, Stauder J, Trauth D, Bassett E, Jurke B, Bönsch C, Gärtner R, Holsten S, Jamal R, Kerzel U, Stautner M (2017) Assisstenzsysteme in der Produktionstechnik. Proceedings of the 29th Aachener Werkzeugmaschinen-Kolloquium (AWK): Aachen May 18th and 19th 2017 Apprimus Verlag, 265–287
49. Shewhart WA (1980) Economic control of quality of manufactured product, Faks. d. Ausg. New York, Van Nostrand, 1931. Quality Press, Milwaukee, Wis
50. Slater P (1977) The measurement of intrapersonal space by grid technique. Dimensions of intrapersonal space Vol. 2. Wiley, London